Regional Impacts of Climate Change and Atmospheric CO_2 on Future Ocean Carbon Uptake: A Multimodel Linear Feedback Analysis

TILLA ROY,* LAURENT BOPP,* MARION GEHLEN,* BIRGIT SCHNEIDER,+ PATRICIA CADULE,* THOMAS L. FRÖLICHER,#,@,& JOACHIM SEGSCHNEIDER,** JERRY TJIPUTRA,++ CHRISTOPH HEINZE,++ AND FORTUNAT JOOS#,@

* *Laboratoire des Sciences du Climat et de l'Environnement, Gif sur Yvette, France*
+ *Institute of Geosciences, Kiel, Germany*
# *Climate and Environmental Physics, Physics Institute, University of Bern, Bern, Switzerland*
@ *Oeschger Centre for Climate Change Research, University of Bern, Bern, Switzerland*
& *Program in Atmospheric and Oceanic Sciences, Princeton University, Princeton, New Jersey*
** *Max Planck Institut für Meteorologie, Hamburg, Germany*
++ *Geophysical Institute, and Bjerknes Centre for Climate Research, Bergen, Norway*

(Manuscript received 14 April 2010, in final form 14 December 2010)

ABSTRACT

The increase in atmospheric CO_2 over this century depends on the evolution of the oceanic air–sea CO_2 uptake, which will be driven by the combined response to rising atmospheric CO_2 itself and climate change. Here, the future oceanic CO_2 uptake is simulated using an ensemble of coupled climate–carbon cycle models. The models are driven by CO_2 emissions from historical data and the Special Report on Emissions Scenarios (SRES) A2 high-emission scenario. A linear feedback analysis successfully separates the regional future (2010–2100) oceanic CO_2 uptake into a CO_2-induced component, due to rising atmospheric CO_2 concentrations, and a climate-induced component, due to global warming. The models capture the observation-based magnitude and distribution of anthropogenic CO_2 uptake. The distributions of the climate-induced component are broadly consistent between the models, with reduced CO_2 uptake in the subpolar Southern Ocean and the equatorial regions, owing to decreased CO_2 solubility; and reduced CO_2 uptake in the mid-latitudes, owing to decreased CO_2 solubility and increased vertical stratification. The magnitude of the climate-induced component is sensitive to local warming in the southern extratropics, to large freshwater fluxes in the extratropical North Atlantic Ocean, and to small changes in the CO_2 solubility in the equatorial regions. In key anthropogenic CO_2 uptake regions, the climate-induced component offsets the CO_2-induced component at a constant proportion up until the end of this century. This amounts to approximately 50% in the northern extratropics and 25% in the southern extratropics and equatorial regions. Consequently, the detection of climate change impacts on anthropogenic CO_2 uptake may be difficult without monitoring additional tracers, such as oxygen.

1. Introduction

Reliable simulations of the evolution of the earth's atmospheric CO_2 concentration and temperature (T) are required to anticipate the impacts of climate change and to set emission targets that minimize the risk of adverse impacts on ecosystems and human society. Including the climate-induced exchanges of CO_2 between terrestrial and ocean carbon reservoirs and the atmosphere (i.e., the climate–carbon cycle feedbacks) in earth system models initiates a positive feedback loop (Meyer et al. 1999; Cox et al. 2000; Friedlingstein et al. 2001; Plattner et al. 2001; Dufresne et al. 2002; Friedlingstein et al. 2006): that is, the global warming decreases the CO_2 uptake by the ocean and terrestrial biosphere and accelerates the rise in atmospheric CO_2 concentrations and global warming. In the coupled climate–carbon cycle model (C^4M) intercomparison project (C^4MIP) (Friedlingstein et al. 2006), eleven coupled climate–carbon cycle models were used to simulate the interactions between the climate system and the carbon cycle over the industrial era. Friedlingstein et al. (2006)

Corresponding author address: Tilla Roy, Laboratoire des Sciences du Climat et de L'Environnement (LSCE), UMR CEA-CNRS-UVSQ, CEN de Saclay/L'Orme des Merisiers, Bât. 712, F-91191 Gif-sur-Yvette CEDEX, France.
E-mail: tilla.roy@lsce.ipsl.fr

DOI: 10.1175/2010JCLI3787.1

demonstrated that the climate–carbon cycle feedbacks cause atmospheric CO_2 concentrations to increase by 20–200 ppm relative to simulations without explicit climate–carbon cycle feedbacks, which induces an additional warming of 0.1°–1°C by 2100 (Meehl et al. 2007). Thus, to stabilize atmospheric CO_2 concentrations, reductions in carbon emissions must be more stringent than if this feedback did not operate (Prentice et al. 2001; Edmonds et al. 2004; Jones et al. 2006; Matthews 2006; Matthews and Keith 2007). A subset of the new generation Intergovernmental Panel on Climate Change (IPCC) models will explicitly take the climate–carbon cycle feedbacks into account to simulate the future co-evolution of atmospheric CO_2 and global warming (http://cmip-pcmdi.llnl.gov/cmip5/).

In Friedlingstein et al. (2006), a linear feedback analysis approach was developed that isolates the impact of rising atmospheric CO_2 concentrations from that of climate change on the cumulated uptake of atmospheric CO_2 by both the ocean and land reservoirs up until the end of this century. It was found that the terrestrial biosphere dominates the magnitude and uncertainty of the global climate–carbon cycle feedback in the majority of the C^4Ms (Friedlingstein et al. 2006). A number of studies have addressed the terrestrial climate–carbon cycle feedbacks in detail (Meyer et al. 1999; Joos et al. 2001; Dufresne et al. 2002; Jones et al. 2003; Cox et al. 2004; Matthews et al. 2005; Matthews et al. 2007). Recently, after observation-based studies revealed that regional ocean carbon sinks can undergo strong variations within several years (Schuster and Watson 2007; Metzl 2009; Schuster et al. 2009; Watson et al. 2009), there has been a renewed interest in the oceanic feedbacks.

Although there has been a relatively long history of investigating the impact of climate change on oceanic CO_2 fluxes (Maier-Reimer et al. 1996; Sarmiento and Le Quéré 1996; Sarmiento et al. 1998; Joos et al. 1999; Matear and Hirst 1999; Plattner et al. 2001), the models used did not include fully interactive carbon cycles. In C^4MIP (Friedlingstein et al. 2006), a linear feedback analysis approach was applied to quantify the global climate–carbon cycle feedback from the ocean in C^4Ms, but regional analyses were not made. Boer and Arora (2010) applied a slightly different feedback analyses approach (Boer and Arora 2009) to determine the geographical distributions of oceanic and terrestrial climate–carbon cycle feedbacks, but most of the process attribution was focused on the larger responses over the terrestrial biosphere. In several C^4M studies (Joos et al. 1999; Plattner et al. 2001; Crueger et al. 2008; Yoshikawa et al. 2008; Frölicher and Joos 2010; Tjiputra et al. 2010), the regional oceanic climate–carbon cycle feedbacks were estimated and attributed to ocean processes (Plattner et al. 2001; Crueger et al. 2008; Yoshikawa et al. 2008), but a linear feedback analysis was not applied.

Here, the linear feedback analysis approach of Friedlingstein et al. (2006) is extended to the regional scale to focus specifically on regional climate–carbon cycle feedbacks from the ocean in a suite of C^4Ms:

(i) Which regions dominate the global climate–carbon cycle feedback from the ocean?
(ii) What processes drive the dominant regional climate–carbon cycle feedbacks and the intermodel variability?
(iii) What are the implications for regional anthropogenic CO_2 uptake?

2. Method

a. Models

All the models are fully coupled, global C^4Ms. A brief description of each model is provided below, and the differences from the simulations of Friedlingstein et al. (2006) are described. The carbon chemistry of the models is based on the Ocean Carbon Model Intercomparison Project (OCMIP2) protocol (Najjar et al. 2007); any relevant deviations from this protocol are listed.

1) IPSL

The L'Institut Pierre-Simon Laplace Coupled Model, version 4 (IPSL CM4)-LOOP model consists of the Laboratoire de Météorologie Dynamique atmospheric model (LMDZ-4), with a horizontal resolution of about $3° \times 3°$ and 19 vertical levels (Hourdin et al. 2006), which is coupled to the Océan Parallélisé (OPA-8) ocean model, with a horizontal resolution of $2° \times 2° \times \cos\varphi$ and 31 vertical levels and the linear inverse model (LIM) sea ice model (Madec et al. 1998). The terrestrial biosphere is represented by the global vegetation model Organizing Carbon and Hydrology in Dynamic Ecosystems (ORCHIDEE; Krinner et al. 2005) and the marine carbon cycle by the PISCES model (Aumont et al. 2003). For more details on PISCES see Aumont and Bopp (2006), Gehlen et al. (2006), and Schneider et al. (2008).

2) NCAR/UBERN

The physical core of the National Center for Atmospheric Research (NCAR) Climate System Model, version 1.4 (CSM1.4; hereafter NCAR) (Fung et al. 2005; Doney et al. 2006; Frölicher et al. 2009; Steinacher et al. 2009; Frölicher and Joos 2010; Steinacher et al. 2010) used for the University of Bern simulations

(UBERN) is a modified version of the NCAR CSM1.4 coupled physical model, consisting of ocean, atmosphere, land, and sea ice components integrated via a flux coupler without flux adjustments (Boville and Gent 1998; Boville et al. 2001). The atmospheric Community Climate Model version 3 (CCM3) is run with a spectral truncation resolution of ~3.75° (T31 grid) and 18 levels in the vertical (Kiehl et al. 1998). The NCAR CSM Ocean Model (NCOM) is non-eddy resolving with 25 vertical levels and a resolution of 3.6° in longitude and 0.8°–1.8° in latitude (T31 × 3 grid) (Gent et al. 1998). The dynamical sea ice model is run at the resolution of the ocean model, and the land surface model is run at the resolution of the atmospheric model. Biogeochemistry is simulated with a modified version of the terrestrial biogeochemistry model Collaborative Adaptive Sensing of the Atmosphere (CASA) (Randerson et al. 1997) and a prognostic version (Doney et al. 2006) of the OCMIP-2 ocean biogeochemistry model.

The time histories of CO_2 from land-use emissions, non-CO_2 greenhouse gases CH_4, N_2O, CFC-11, and CFC-12, other halogenated species, SF_6, and spatially explicit aerosol loading from explosive volcanism and anthropogenic sulfate aerosols, and recurring annual cycles of ozone and natural sulfate aerosols have also been included in the NCAR model. For further details see Frölicher et al. (2009).

3) BCM-C

The Bergen earth system model (BCM-C) is an extension of the Bergen Climate Model (Furevik et al. 2003) and consists of the spectral atmospheric general circulation model Action de Recherche Petite Echelle Grande Echelle (ARPEGE) from Météo-France (Deque et al. 1994) and an ocean component based on the Miami Isopycnic Coordinate Ocean Model (MICOM) (Bleck et al. 1992). ARPEGE is run at a horizontal resolution of about 2.8° × 2.8° with 31 vertical levels between the surface to 0.01 hPa (20 levels in the troposphere). The representation of most model variables in ARPEGE is spectral (i.e., scalar fields are decomposed on a truncated basis of spherical harmonic functions). MICOM has a time step of 4800 s and a stack of 34 vertical isopycnic layers, with potential densities ranging from 1029.514 to 1037.800 kg m^{-3}. A non-isopycnic surface mixed layer provides the linkage between the atmospheric forcing and the ocean interior. Incremental remapping is used and is adapted to the grid staggering of MICOM for tracer advection and layer thickness, which ensures monotonicity of the tracers. The terrestrial biosphere is represented by the Lund–Postdam–Jena Model (LPJ) (Sitch et al. 2003) and the marine carbon cycle by the Hamburg Ocean Carbon Cycle model (HAMOCC5.1; Maier-Reimer 1993; Maier-Reimer et al. 2005). For more details on BCM-C see Tjiputra et al. (2010).

4) MPIM

The earth system model employed at the Max Planck Institute for Meteorology (MPIM) consists of the ECHAM5 atmospheric model (Roeckner et al. 1996) with 31 vertical levels, the Jena Scheme for Biosphere–Atmosphere coupling in Hamburg (JSBACH) terrestrial biosphere model, and the MPIOM physical ocean model. MPIOM includes a sea ice model (Marsland et al. 2003) and the HAMOCC5.1 marine biogeochemistry model (Maier-Reimer et al. 1993; Six and Maier-Reimer 1996; Maier-Reimer et al. 2005). The coupling of the marine and atmospheric model components and the carbon cycles is achieved using the OASIS coupler. HAMOCC5.1 is implemented into the MPIOM physical ocean model configuration using a curvilinear coordinate system with a 1.5° nominal resolution, where the North Pole is placed over Greenland and provides relatively high horizontal resolution in the Nordic Seas. The vertical resolution is 40 layers, with higher resolution in the upper part of the water column (10 m at the surface to 13 m at 90 m). The carbonate chemistry is identical to the one described in Maier-Reimer (1993). For more HAMOCC5.1 details see Maier-Reimer et al. (2005) and Schneider et al. (2008).

b. Model simulations

The models are forced using the same CO_2 trajectory: CO_2 emissions from historical (1860–1999) data (Marland and Andres 2005) and the Special Report on Emissions Scenarios (SRES) A2 future (2000–2100) scenario (Nakicenovic et al. 2000). Two transient simulations (1860–2100) of each C^4M are performed. The coupled simulation is the standard simulation with a fully interactive carbon cycle and global warming. In the uncoupled simulation, global warming is limited by fixing the atmospheric CO_2 to the preindustrial value in the radiation transfer code, while still allowing both atmospheric pCO_2 to rise in response to anthropogenic CO_2 emissions and exchanges between atmospheric, marine, and terrestrial carbon reservoirs (Friedlingstein et al. 2006). The only anthropogenic forcing in the simulations is fossil CO_2, except in NCAR (see above). The influence of the drift in the tracer fields is cancelled when calculating the climate-induced component from the difference between the coupled and uncoupled simulations—assuming that both simulations have identical drifts. Note the NCAR tracer fields have been drift corrected.

c. *Climate–carbon cycle feedback analysis*

On decadal time scales the change in the total carbon stored by the ocean ΔC_O is equivalent to the time-integrated flux of CO_2 across the air–sea interface F_O,

$$\Delta C_O = \int F_O \, dt. \tag{1}$$

Here, the linear feedback analysis approach of Friedlingstein et al. (2006) is applied to tease apart the regional changes in ΔC_O, (i.e., 2010–2100) into CO_2-induced components that are driven by rising global atmospheric CO_2 concentrations ΔC_{CO2} and climate-induced components that are driven by climate change, ΔC_{CLIM}.

This approach rests on three key assumptions. First, ΔC_O can be approximated by a linear combination of these two responses:

$$\Delta C_O = \Delta C_{CO2} + \Delta C_{CLIM}. \tag{2}$$

Second, ΔC_{CO2} is proportional the change in globally averaged atmospheric CO_2 concentration, ΔC_A,

$$\Delta C_{CO2} = \beta \Delta C_A, \tag{3}$$

where β is the sensitivity parameter of the cumulated oceanic CO_2 uptake to atmospheric CO_2. Third, ΔC_{CLIM} is proportional to climate change, where the change in global near-surface atmospheric temperature ΔT is used as a proxy of climate change

$$\Delta C_{CLIM} = \gamma \Delta T, \tag{4}$$

and γ is the sensitivity parameter of the cumulated oceanic CO_2 uptake to climate change.

That is,

$$\Delta C_O = \beta \Delta C_A + \gamma \Delta T. \tag{5}$$

To estimate ΔC_{CO2} and ΔC_{CLIM} we require two simulations: the coupled and uncoupled simulations (section 2b). The superscripts "C" and "U" refer to quantities from the coupled and uncoupled simulations respectively. For the uncoupled simulation, ΔT^U is small since climate change due to rising atmospheric CO_2 has been suppressed—there is some warming due to CO_2-induced changes in the terrestrial biosphere (Matthews 2007)—and Eq. (5) reduces to

$$\Delta C_O^U \approx \beta^U \Delta C C_A^U. \tag{6}$$

From this relationship (e.g., Fig. 1a), β^U, the slope, is determined by linear regression. For the coupled simulation, we assume that $\beta^C \approx \beta^U$. Such that

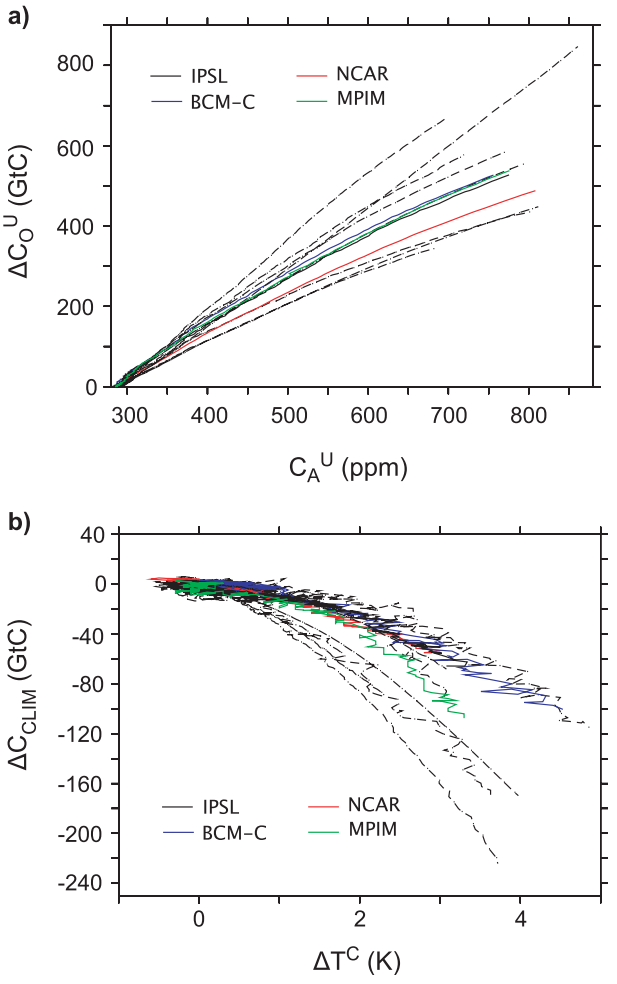

FIG. 1. (a) The global change in cumulated (1860–2100) oceanic CO_2 uptake (PgC) ΔC_O^U vs the global-mean annual-mean atmospheric pCO_2 (ppm) ΔC_A^U from the "uncoupled" C^4M simulations of Friedlingstein et al. (2006)—see Eq. (6). The gradient of the relationship represents the global sensitivity of oceanic CO_2 uptake to rising atmospheric CO_2 concentrations β^U (PgC ppm^{-1}). (b) The global change in climate-induced cumulated (1860–2100) oceanic CO_2 uptake (PgC) ΔC_{CLIM} vs the global-mean annual-mean change in surface atmospheric temperature (K) ΔT^C from the "coupled" C^4M simulations of Friedlingstein et al. (2006)—see Eq. (8). The gradient of the relationship represents the global sensitivity of the CO_2 uptake to climate change γ (PgC K^{-1}). In both panels, the models used in this study are highlighted in color and include an additional model, BCM-C, not included in the original study of Friedlingstein et al. (2006).

$$\Delta C_O^C = \beta^U \Delta C_A^C + \gamma \Delta T^C, \tag{7}$$

which rearranges to

$$\Delta C_{CLIM} = \gamma \Delta T^C. \tag{8}$$

From this relationship (e.g., Fig. 1b), γ is approximated by linear regression.

The success of this approach essentially depends on β^U: if Eq. (6) is sufficiently linear (as in Fig. 1a) then ΔC_O can be separated into the components ΔC_{CO2} and ΔC_{CLIM}. If the relationships between ΔC_{CLIM} and ΔT^C deviate from linearity (as in Fig. 1b), this does not influence our estimates of ΔC_{CO2} and ΔC_{CLIM}; these terms are calculated independently of γ, that is,

$$\Delta C_{\mathrm{CLIM}} = \Delta C_O^C - \beta \Delta C_A^C. \quad (9)$$

Here, the same approach is applied both spatially and regionally. The regional sensitivity parameters are calculated by first integrating the CO_2 fluxes over each region. For a direct comparison with the regional estimates of anthropogenic CO_2 uptake from the ocean inversions (Mikaloff-Fletcher et al. 2006; Jacobson et al. 2007; Gerber et al. 2009; Gruber et al. 2009; Gerber and Joos 2010) the same regions have been used here. All regional regressions are performed over the period 2010–2100. Since we are interested in isolating the long-term trends in CO_2 storage by the ocean and the processes that drive them, the model data have been smoothed with a 10-yr running mean.

d. Evaluation of the C⁴M simulations

We evaluate some key aspects of the coupled C⁴M simulations over the historical period (1985–2005). For further model validation see Schneider et al. (2008) for IPSL, NCAR, and MPIM—and Tjiputra et al. (2010) for BCM-C. Temperature and salinity (S) distributions are in good agreement with climatological data from the *World Ocean Atlas* (Conkright et al. 2002; Collier and Durack 2006), indicating a reasonable reproduction of the large-scale features of ocean circulation (Fig. 2). Phosphate concentrations have high spatial correlations (R = 0.7–0.9), masking a positive offset in MPIM and NCAR that is caused by excessive iron limitation of biological production (Schneider et al. 2008; Steinacher et al. 2010). The simulated yearly maximum mixed-layer depths (MLD_{max}) correlate weakly with climatological data from Boyer-Montegut et al. (2004); distinctly higher correlations are found when including the seasonal MLD (Schneider et al. 2008).

The spatial patterns of simulated annual-mean ΔpCO_2 (sea–air; Fig. 3) resemble the observation-based climatology (Takahashi et al. 2009), with high ΔpCO_2 in the tropics. Regions of oceanic CO_2 uptake are found in the northern mid and high latitudes and in the southern midlatitudes. In the Southern Ocean, around 60°S, the models largely fail to reproduce the low positive ΔpCO_2 values, which were recently diagnosed from the latest ΔpCO_2 climatology and attributed to the release of respiratory CO_2 that accumulates below the sea ice during winter

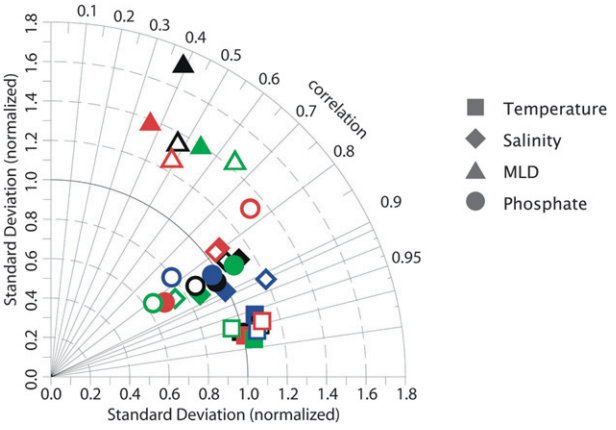

FIG. 2. A Taylor diagram of several key circulation diagnostics in the coupled C⁴M simulations: T, S, MLD, and phosphate (PO_4). The filled symbols represent the 3D annual average; except MLD, which is the maximum monthly average. The unfilled symbols are seasonally varying surface fields; except for the phosphate which is averaged between 0–100 m. The simulated fields are evaluated against T, S, and PO_4 observations are from the *World Ocean Atlas* (Conkright et al. 2002; Collier and Durack 2006) and the MLD from Boyer-Montegut et al. (2004). The MLDs for MPIM are not shown in the diagram because the normalized standard deviations are out of range (Schneider et al. 2008). This figure is an extension of the Fig. 1 in Schneider et al. (2008); it now also includes the BCM-C model.

(Takahashi et al. 2009). Nevertheless, the models have correlations on the order of 0.3–0.65 to the observation-based annual-mean ΔpCO_2 (Fig. 4), which are higher than the correlations to the previous climatology (Takahashi et al. 2002). When including the seasonal cycle of ΔpCO_2, the strength of the correlations increases in all models except in MPIM, which overestimates the seasonal amplitude of ΔpCO_2 in the extratropics (not shown).

3. Results

The linear feedback analysis can be applied successfully not only at the global scale but also regionally and spatially. By applying the linear feedback approach at the regional scale, the component of the change in the future cumulated CO_2 uptake (2010–2100) due to climate change, ΔC_{CLIM}, has been isolated from the change in cumulated CO_2 uptake due to rising atmospheric CO_2 concentrations, ΔC_{CO2} (Tables 1 and 2; Fig. 5).

The global CO_2-induced component of the cumulated CO_2 uptake (2010–2100) ΔC_{CO2} ranges between 141 and 187 PgC (Table 1), with most of the uptake occurring in the subpolar Southern Ocean and the equatorial regions in all models (Fig. 5). The global climate–induced component of the cumulated CO_2 uptake (2010–2100) ΔC_{CLIM} ranges between −29 and −50 PgC (Table 2).

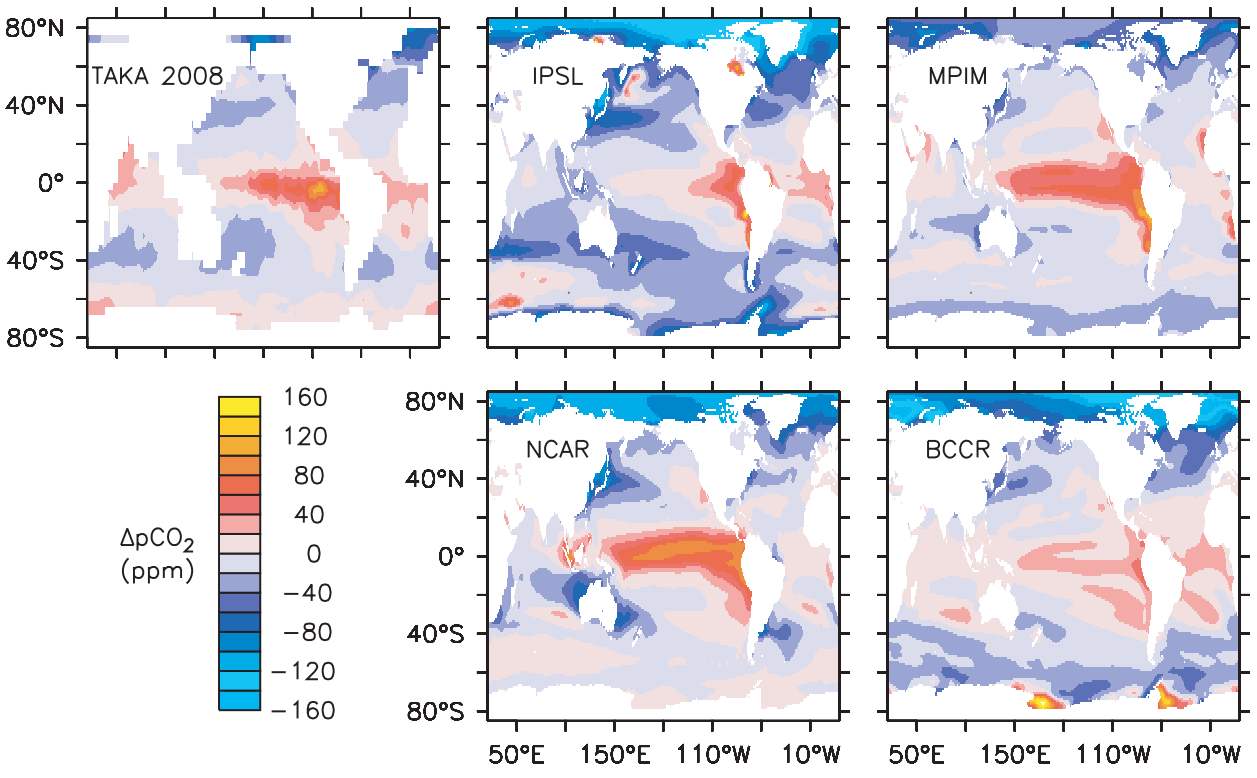

FIG. 3. The sea–air CO_2 partial pressure difference (ΔpCO_2) from observation-based estimates (Takahashi et al. 2009) and the coupled C^4M simulations (1985–2005). A negative ΔpCO_2 indicates an oceanic uptake of atmospheric CO_2.

The regions that dominate the climate-induced change in uptake vary between the models (Table 2; Fig. 5).

The magnitudes of the global CO_2-induced sensitivities β of the four C^4Ms are similar (ca. 1.1 PgC ppm^{-1}) except for NCAR, which is 0.2 PgC ppm^{-1} lower (Table 3). The magnitudes of the global climate-induced sensitivities γ are similar (~ -20 PgC K^{-1}), except for BCM-C which is -30 PgC K^{-1} (Table 3).

The zonally averaged distributions of β are broadly consistent between the models with the largest βs in the high latitudes of both the northern and southern hemispheres (Fig. 6a), as are the zonal distributions of γ (Fig. 6b), with positive γs in the Arctic and the Antarctic and negative γs elsewhere. On average, the regions with the highest βs are the North Atlantic and the Southern Ocean (Fig. 7a). The North Atlantic and the midlatitude Southern Ocean have the largest negative γs, while the Arctic and the polar Southern Ocean have positive γs (Fig. 7b).

4. Discussion

a. CO_2-induced sensitivity of oceanic CO_2 uptake, β

The CO_2-induced sensitivity parameter β is a measure of how much the cumulated CO_2 uptake by the ocean changes in response to an increase in atmospheric pCO_2. The more confident we are in the estimate of β, the more effectively we can isolate the change in the future cumulated CO_2 uptake by the oceans due to climate change in the C^4M simulations [i.e., Eq. (6) must be sufficiently linear regionally].

Despite the expected deviations from linearity due to the reduction in the buffer capacity of the ocean, the relationships between CO_2-induced cumulated CO_2 uptake and atmospheric CO_2 are linear in all oceanic regions (Fig. 8) and at all grid points where CO_2 uptake is significant throughout the global ocean. The buffer capacity is highest in warmer waters, and it is also in these regions that a reduction in the buffer capacity is expected to have the most impact on the oceanic CO_2 uptake (Sabine et al. 2004). However, no significant regional differences are apparent (cf. Fig. 8b to Fig. 8d). For the purpose of isolating the climate impact on cumulated CO_2 uptake using the linear feedback analysis approach, changes in the buffer capacity have little impact on the cumulated CO_2 uptake over the twenty-first century. By focusing only on the future period of 90 years the relationship approximates linearity (cf. Fig. 1a to Figs. 8a–d).

The regional relationships between ΔC_{CLIM} and ΔT^C deviate from linearity (Figs. 8e–h)—as in the global feedback analysis (Friedlingstein et al. 2006). However,

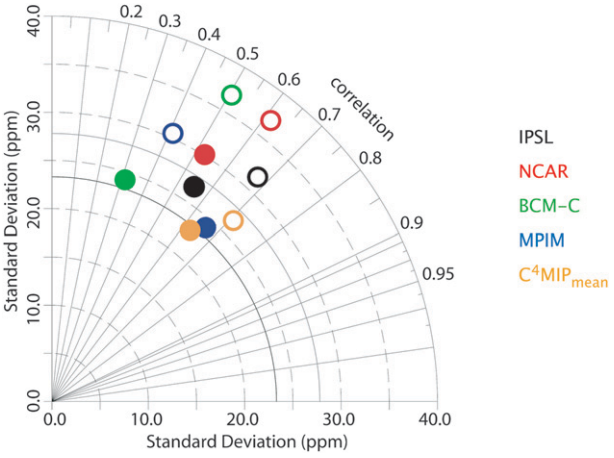

FIG. 4. A Taylor diagram of ΔpCO_2 in the coupled C^4M simulations. The simulated fields are correlated to the ΔpCO_2 observations of Takahashi et al. (2009). The filled symbols are annual-mean 2D fields, and the unfilled symbols are seasonally varying 2D surface fields. The black line (at about 23 ppm) corresponds to the standard deviation of the observation-based annual-mean ΔpCO_2 (Takahashi et al. 2009); the gray line (at around 28 ppm) corresponds to the observation-based seasonally varying ΔpCO_2 (Takahashi et al. 2009).

this also does not hamper our ability to separate ΔC_{CLIM} from ΔC_{CO2} (section 2c).

1) GLOBAL β

The similarities of the global β are remarkable, with three of the models having β magnitudes of approximately 1.1 PgC ppm^{-1} (Table 3). In Friedlingstein et al. (2006), the models have a narrower range of ocean CO_2-induced sensitivities, β_O (i.e., 0.8–1.5 PgC ppm^{-1}), than land CO_2-induced sensitivities, β_L, (i.e., 0.2–2.8 PgC ppm^{-1}). This probably reflects the strong observational constraints (temperature, salinity, and also nutrients, CFCs, ^{14}C etc.) that are routinely used to evaluate the dynamics and the anthropogenic CO_2 uptake in global biogeochemical ocean circulation models (Levitus 1982; Levitus et al. 1993; Levitus and Boyer 1994; Levitus et al. 1994; Conkright et al. 2002; Dutay et al. 2002; Key et al. 2004; Matsumoto et al. 2004; Sabine et al. 2004). Arguably, the comparable constraints on the CO_2 uptake over land are more uncertain.

The magnitude of global β is correlated to the global mean MLD (Fig. 9) in agreement with Mignone et al. (2006). Mignone et al. (2006) demonstrated an increase in anthropogenic CO_2 uptake when the pycnocline was deepened by systematically increasing the strength of the Southern Hemisphere winds. When focusing only on the four models used in this study, the relationship is less convincing (i.e., although the models have a similar global β, they have different mixed-layer depths).

Although the greater sea ice coverage in the polar regions in the NCAR model limits anthropogenic CO_2 uptake in these regions (Fig. 10f) and contributes to the lower global β of the NCAR model, it is expected that ocean circulation processes are the dominant cause of the differences in both global and regional β—see the influence of Ekman transport (Mignone et al. 2006; Ito et al. 2010) and seasonal and mesoscale variability (Lachkar et al. 2009) on anthropogenic CO_2 uptake. The intermodel differences in global β can also not be explained by differences in the strength of the Atlantic meridional overturning circulation (AMOC); the IPSL model has a lower initial AMOC than the other models (Table 4), yet it has a similar global β. With the limited selection of diagnostics available, a more detailed analysis of the impact of circulation on cumulated CO_2 uptake is beyond the scope of this study.

2) COMPARISON OF β WITH OBSERVATIONS

An observation-based estimate of global β (i.e., β_{obs} = 1.5 ± 0.3 PgC ppm^{-1}) is made using the anthropogenic

TABLE 1. The zonally integrated future (2010–2100) cumulated CO_2 uptake (PgC) due to rising atmospheric CO_2 concentrations (ΔC_{CO2}). The regional CO_2 uptakes are listed in parentheses as a percentage of the global cumulated CO_2 uptake. A positive cumulated CO_2 uptake is a flux of atmospheric CO_2 into the ocean.

		ΔC_{CO2} (PgC)				
Zonal regions	Latitude band	IPSL	NCAR	BCM-C	MPIM	Ensemble mean ± std dev
Polar Southern Ocean	>58°S	27.0 (15)	20.5 (15)	20.2 (11)	23.2 (13)	22.7 ± 2.7 (13)
Subpolar Southern Ocean	44°–58°S	35.9 (20)	28.7 (20)	41.3 (22)	36.6 (21)	35.6 ± 4.5 (21)
Southern midlatitudes	18°–44°S	32.5 (18)	18.7 (13)	32.2 (17)	25.8 (15)	27.3 ± 5.7 (16)
Equatorial	18°S–18°N	43.1 (24)	42.8 (30)	50.7 (27)	59.5 (34)	49.0 ± 6.8 (29)
Northern midlatitudes	18°–49°N	24.2 (14)	22.5 (16)	28.8 (15)	22.1 (13)	24.4 ± 2.7 (14)
Northern high latitudes*	49°–76°N	14.2 (8)	6.6 (5)	12.0 (6)	9.3 (5)	10.5 ± 2.8 (6)
Arctic Basin**	>76°N**	1.4 (1)	1.5 (1)	1.4 (1)	0.0 (<0)	1.1 ± 0.6 (1)
Total		178.3	141.3	186.7	176.6	170.7 ± 17.4

* Here, the region called Arctic in Figs. 5, 10, and 11 is split into northern high latitudes and the Arctic Basin. See next note.
** The latitude limit of the Arctic Basin in the Pacific sector is the Bering Strait (and is shown in Fig. 7).

TABLE 2. The zonally integrated future (2010–2100) cumulated CO_2 uptake (PgC) due to climate change (ΔC_{CLIM}). See Table 1 for details.

Zonal regions	Latitude band	ΔC_{CLIM} (PgC)				
		IPSL	NCAR	BCM-C	MPIM	Ensemble mean ± std dev
Polar Southern Ocean	>58°S	4.2 (−10)	−2.1 (7)	5.1 (−10)	−2.2 (5)	1.3 ± 3.4 (−3)
Subpolar Southern Ocean	44°–58°S	−5.1 (12)	−5.0 (17)	−13.3 (26)	−12.3 (27)	−8.9 ± 3.9 (21)
Southern midlatitudes	18°–44°S	−11.3 (27)	−4.1 (14)	−12.5 (25)	−5.0 (11)	−8.3 ± 3.8 (20)
Equatorial	18°S–18°N	−7.2 (17)	−6.8 (23)	−13.9 (28)	−15.3 (33)	−10.8 ± 3.9 (26)
Northern midlatitudes	18°–49°N	−15.4 (37)	−8.0 (28)	−9.2 (18)	−9.2 (20)	−10.4 ± 2.9 (25)
Northern high latitudes	49°–76°N	−7.4 (18)	−3.3 (11)	−6.3 (13)	−3.8 (8)	−5.2 ± 1.7 (13)
Arctic Basin	>76°N	0.9 (−2)	0.4 (−1)	−0.2 (<0.1)	2.0 (-4)	0.8 ± 0.8 (−2)
Total		−41.2	−28.8	−50.3	−45.8	−41.5 ± 8.0

CO_2 uptake estimate (i.e., 118 ± 19 PgC for 1820–1994) and the change in atmospheric pCO_2 since the preindustrial era (i.e., 78 ppm) from Sabine et al. (2004), which includes an unknown perturbation due to climate change. An analogous model-based estimate ($\beta = 1.3 \pm 0.2$ PgC ppm^{-1}) is made using the change in cumulated CO_2 uptake (1860–1994) from the coupled simulation and is within the range of the observation-based estimate. Also, the zonal distribution of ΔC_{CO2} (Fig. 5) closely resembles the historical anthropogenic CO_2 flux from inversion studies (Mikaloff-Fletcher et al. 2006; Jacobson et al. 2007; Gerber et al. 2009) and forward modeling studies (Orr et al. 2001), with the dominant CO_2 uptake regions in the subpolar Southern Ocean and the equatorial Pacific (cf. Fig. 5 with the analogous Fig. 9 in Mikaloff-Fletcher et al. 2006 and Fig. 2a in Gerber et al. 2009). These similarities give us confidence that the models are capturing the global and regional responses of the oceanic CO_2 uptake to rising atmospheric CO_2 concentrations.

b. *Climate-induced sensitivity of oceanic CO_2 uptake γ*

The climate-induced sensitivity parameter γ is a measure of how much the cumulated CO_2 storage by the ocean changes in response to global warming. All models simulate a reduction in the global cumulated CO_2 sink owing to climate change (Table 2)—that is, all models have negative global γs (Table 3). This reduction in oceanic CO_2 uptake causes a positive feedback on atmospheric CO_2 concentrations and implies a subsequent increase in atmospheric temperature.

1) GLOBAL γ

The magnitude of γ reflects changes in a complex set of interacting factors including sea ice coverage, ocean circulation, biological production, and CO_2 solubility, and the relative importance of these factors varies regionally. Globally, the γ of the BCM-C model has a larger magnitude than the other three models (Table 3). This difference is attributed to the much greater local warming in the subpolar Southern Ocean (Fig. 11e) and possibly also due to a reduction in export production (Fig. 11d). The reduction in export production in the subpolar Southern Ocean is a result of the large increase in export production in the surface waters of the polar Southern Ocean as sea ice retreats and alleviates the light limitation on photosynthesis (Steinacher et al. 2010). Although the global atmospheric temperature increases less in BCM-C than in the IPSL and MPIM models (see horizontal axis of Figs. 8e–h), the local climate-induced reduction in CO_2 uptake in the subpolar Southern Ocean (Fig. 8h) dominates the global γ. Since BCM-C is the only isopycnic model, it is expected that it will behave differently—particularly in the higher latitudes.

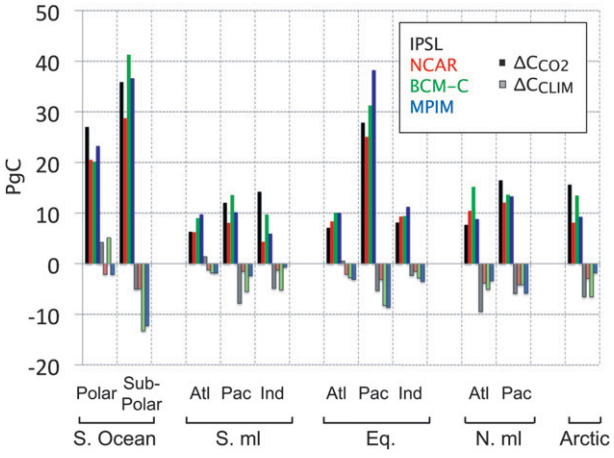

FIG. 5. Regionally integrated cumulated CO_2 uptake (PgC) to the end of this century (2010–2100) in the C^{4}Ms. Here, ΔC_{CO2} (PgC) is represented by the strong color bars, and ΔC_{CLIM} (PgC) is represented by the pale color bars. The coordinates of the regions are identical to Mikaloff-Fletcher et al. (2006): Southern Ocean (S. Ocean; Polar, >58°S; Subpolar, 44°–58°S), Southern midlatitudes (S. ml; 18°–44°S), equatorial (Eq.; 18°S–18°N), Northern midlatitudes (N. ml; 18°–49°N), and Arctic (>49°N).

TABLE 3. The global sensitivity parameter magnitudes α (K ppm^{-1}), β (GtC ppm^{-1}), and γ (GtC K^{-1}) calculated using the same approach of Friedlingstein et al. (2006) for the 1860–2100 period. Note that the gradients of the relationships plotted in Figs. 1a and 1b represent the global β and γ listed in this table.

Model	α (K ppm^{-1})	β (GtC ppm^{-1})	γ (GtC K^{-1})
IPSL	0.0072	1.1	−16
NCAR	0.0046	0.9	−17
BCM-C	0.0055	1.1	−33
MPIM	0.0082	1.1	−22

2) REGIONAL γ

The zonal distributions of γ are broadly consistent between the models and the key features can be explained. In the equatorial regions, the negative γs reflect a reduction in solubility (Fig. 11c) as sea surface temperatures rise (Fig. 11e), while the negative γs (i.e., reduced CO_2 uptake) in the midlatitudes and subpolar Southern Ocean are primarily driven by reduced CO_2 solubility (Fig. 11c) and increased stratification (as diagnosed by the reduction in mixed-layer depth, Fig. 11b). The reduced uptake is partly offset by an increased uptake in the polar regions where all models simulate positive γs (Fig. 6b) that are partly associated with a reduction in the fractional sea ice coverage (Fig. 11f).

The extent to which intermodel differences in ocean properties are reflected in intermodel differences in γ provides an indication of the key ocean processes governing the climate-induced response of CO_2 uptake. But there are two important sources of intermodel and interregional variability in γ (and β) that we can not assess in these simulations. First, the locations of the water masses and fronts are different between the models and they move with climate change—using fixed regions combines regions with very different physical and biogeochemical characteristics, which makes process attribution challenging. Second, there are complex ocean circulation processes that cannot be resolved using the available circulation diagnostics. Nevertheless, a qualitative model intercomparison of changes in mixed-layer depths, sea ice convergence, sea surface temperature and salinity, CO_2 solubility, and export production provides useful insights.

In the northern polar region (>49°N), all the γs are negative (Fig. 11a) owing to both a reduction in CO_2 solubility (Fig. 11c) and an increase in stratification, as diagnosed by the maximum mixed-layer depths (Fig. 11b). The large intermodel variability in sea ice coverage (Fig. 11f) produces larger intermodel variability in the CO_2 solubility compared to other oceanic regions (Fig. 11c); in models which have more sea ice melting—such as BCM-C in the polar Southern Ocean and MPIM in the Arctic—insolation into the surface ocean increases with the ice–albedo feedback leading to a greater reduction in solubility. In the Arctic Basin (>76°N), the γs are positive (Fig. 5b), in agreement with projected changes based on observations of subsurface dissolved inorganic carbon (DIC) concentrations (Bates et al. 2006).

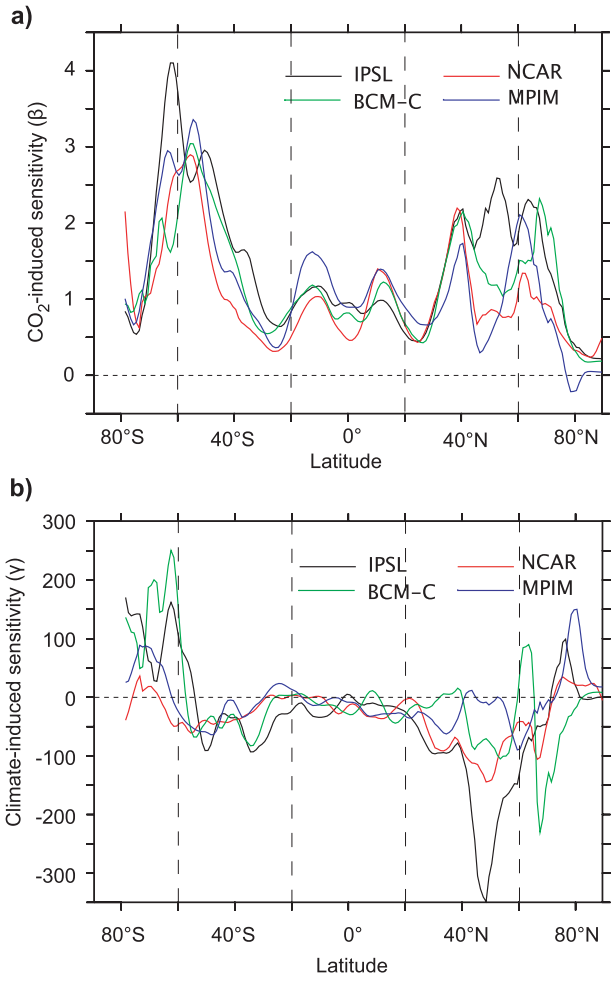

FIG. 6. The zonally averaged sensitivities of the future CO_2 uptake (2010–2100) in the C^{4}M models: (a) β (gC ppm^{-1} m^{-2}) and (b) γ (gC K^{-1} m^{-2}).

In the southern polar regions, the intermodel differences in the γs (Fig. 11a) largely reflect changes in the mixed-layer depth (Fig. 11b); models in which the mixed-layer depths increase are associated with an increased cumulative CO_2 uptake (i.e., positive γs) and vice versa for models in which the mixed-layer depths decrease. The changes in mixed-layer depth in the MPIM model are much greater than in the other models (Fig. 11b), yet they are not associated with large negative γs. The deep mixed layers in MPIM (Fig. 10b) indicate a particularly high level of convective mixing

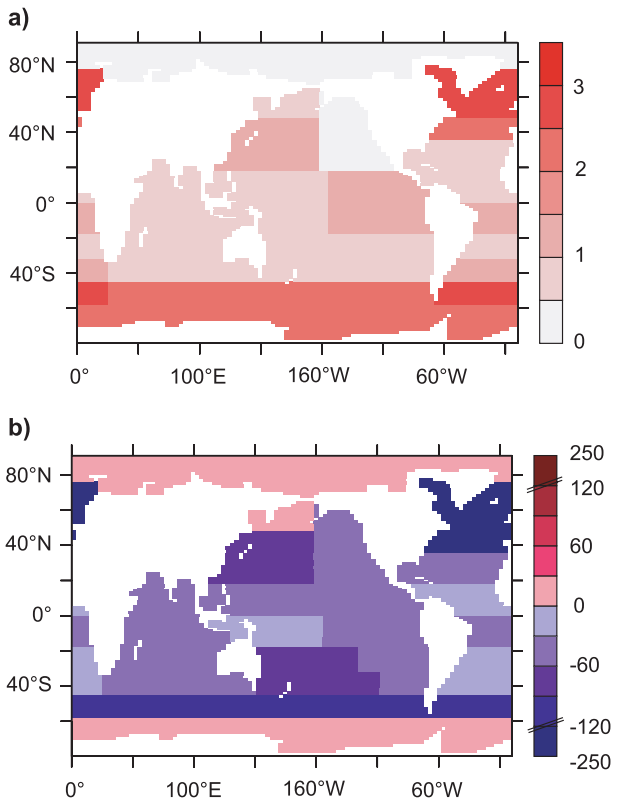

FIG. 7. The ensemble mean (4 C^{4}M models) of the regional sensitivities of the future CO_2 uptake (2010–2100): (a) β (gC ppm^{-1} m^{-2}) and (b) γ (gC K^{-1} m^{-2}).

in the Southern Ocean. Since a well-mixed water column tends to have small vertical gradients in dissolved inorganic carbon, perturbations to the mixed-layer depth would not be expected to drive a large influx of atmospheric CO_2. The extremely large increase in export production in the BCM-C model (Fig. 9d) is not reflected in an equally large change in γ. Hence, around Antarctica, as in the Arctic, the γs are positive (Fig. 5b) where the retreat of sea ice exposes old waters to the atmosphere.

In the subpolar Southern Ocean, the intermodel differences in γ (Fig. 11a) largely reflect differences in solubility (Fig. 11c), in agreement with Sarmiento et al. (1998) and Matear and Hirst (1999). Here, large changes in mixed-layer depths have little impact on the magnitude of γ (e.g., BCM-C and NCAR). Differences in Ekman upwelling due to changes in the wind stress could contribute to intermodel differences in this region but cannot be diagnosed here.

In the midlatitudes, the intermodel differences in the γs (Fig. 11a) reflect changes in both the ocean stratification, as diagnosed by the maximum mixed-layer depth (Fig. 11b), and local warming (Fig. 11e). For example, the maximum mixed-layer depth of the IPSL model decreases significantly more than in the other models in the northern midlatitude Atlantic because of more sea surface freshening (Fig. 11g) and increases in the midlatitude southern Atlantic (Fig. 11b). This produces the expected differences in the regional γs of the IPSL model; that is, a larger negative γ in the northern midlatitude Atlantic, where shallower mixing reduces the efficiency of the anthropogenic CO_2 transport to the deeper ocean and a positive γ in the southern midlatitudes (Fig. 11a).

Several factors could contribute to the anomalous behavior of the IPSL model in the North Atlantic. First, the parameterization of ice calving in the model (Marti et al. 2009) produces a flux of freshwater from the polar ice sheets to the surface Atlantic and Arctic oceans as atmospheric temperatures rise. Second, the reduction in the AMOC rate (Table 4) results in a more sluggish transport of high-salinity waters into the North Atlantic from the south relative to the other models, producing a relative freshening of surface waters in the region. In studies based on results from only one model, the climate-driven reductions in oceanic CO_2 uptake in North Atlantic have been associated with AMOC slow downs (Crueger et al. 2008; Yoshikawa et al. 2008). This study suggests that the AMOC slow down is not the dominant driver; the IPSL and BCM-C models have similar percentage reductions in AMOC (Table 4), yet the IPSL model has a much greater γ (Fig. 11a). Previous studies (Sarmiento et al. 1998; Joos et al. 1999; Swingedouw et al. 2007) have also shown that the AMOC slow down has only a modest impact on the CO_2 flux within this century.

In the equatorial regions, the intermodel differences in γ (Fig. 11a) largely mirror differences in solubility (Fig. 11c), except in the IPSL model in the Atlantic, where increased salinity (Fig. 11g) drives an increase in the mixed-layer depth and cumulated CO_2 uptake. Note that, although changes in export production with climate change are relatively large in the equatorial region, the intermodel differences in export production appear to have little impact on γ. The small changes in nutrient concentrations simulated in these same models (Steinacher et al. 2010) are also indicative of small changes in the CO_2 flux owing to shifts in export production.

c. *Implications for the anthropogenic CO_2 uptake by the ocean*

1) THE DOMINANT CLIMATE-INDUCED CARBON UPTAKE REGIONS

The equatorial regions, the subpolar Southern Ocean, and the midlatitudes of both hemispheres contribute,

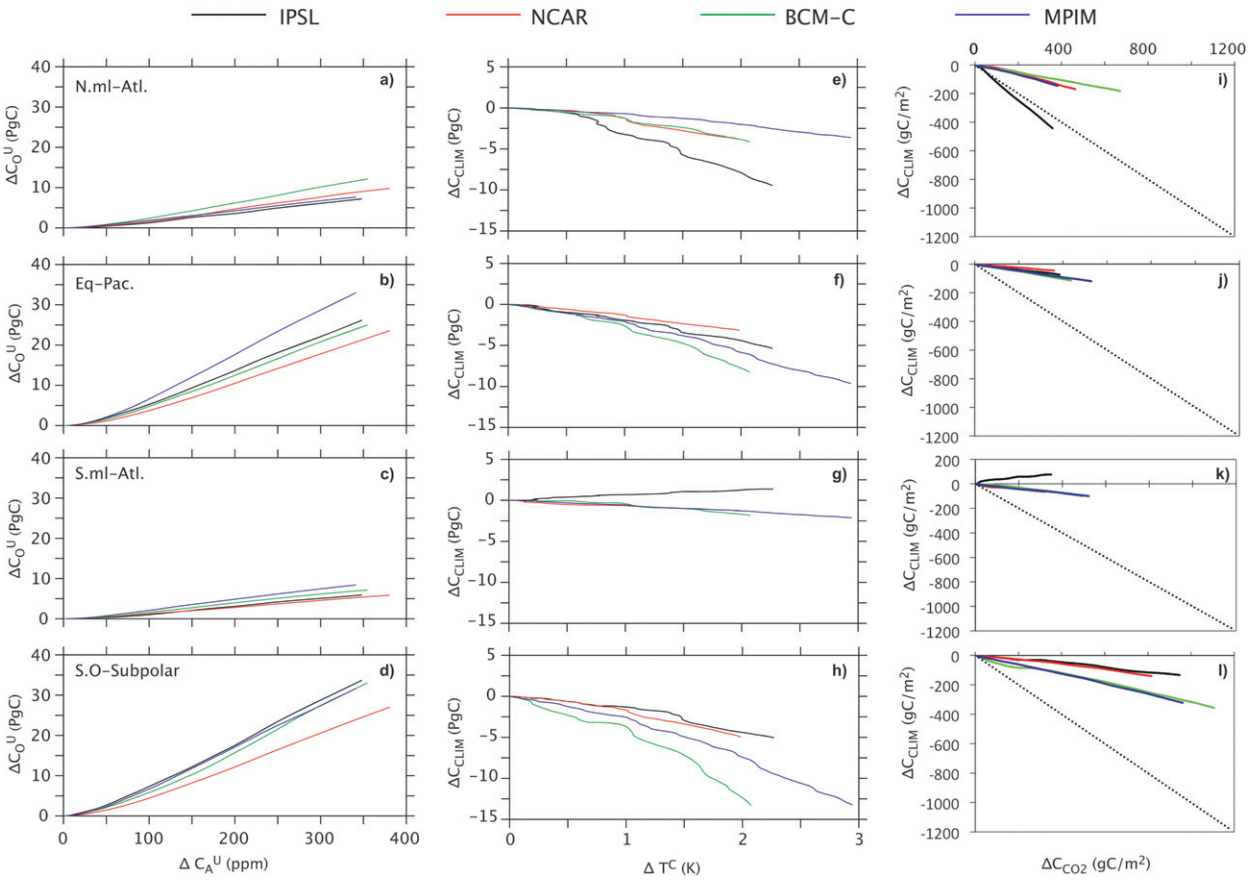

FIG. 8. The relationships for ocean regions where climate change has a significant impact on the cumulated oceanic uptake of CO_2 in C^4M models between 2010–2100: (a)–(d) ΔC_O^U (PgC) vs the change in global-mean annual mean atmospheric pCO_2 ΔC_A^U (ppm), where the gradient represents the regional β [Eq. (6)]. (e)–(h) The ΔC_{CLIM} (PgC) vs the change in the global-mean annual-mean atmospheric temperature ΔT^C (K), where the gradient represents the regional γ [Eq. (8)]. (i)–(l) The time evolution of regional relationship between ΔC_{CLIM} (gC m^{-2}) and ΔC_{CO2} (gC m^{-2}) where the dashed line represents the 1:1 line where the impact of climate change would cancel the increase in uptake due to rising atmospheric CO_2 concentrations. The regions are the northern midlatitude Atlantic (N.ml-Atl), equatorial Pacific (Eq-Pac.), southern midlatitude Atlantic (S.ml-Atl), and the subpolar Southern Ocean (S.O-Subpolar).

on average, between 20%–30% to the global climate–induced change in cumulated CO_2 uptake ΔC_{CLIM} (Table 2). The zone contributing most to global ΔC_{CLIM} is model dependent; for example, in the IPSL model the midlatitudes dominate, while in the other models the equatorial regions are important with variable contributions from the northern and southern extratropics (Table 2).

The intermodel differences in ΔC_{CLIM} are highest from the equatorial regions to Antarctica (Table 2). In the equatorial region, small intermodel differences in γ (Fig. 11a) are amplified in ΔC_{CLIM} (Table 2) when integrating over the large surface area of this zone. Some of the largest differences in the magnitude of γ occur in the southern midlatitudes and the subpolar Southern Ocean (Fig. 11a), where they also translate into large differences in ΔC_{CLIM} (Fig. 5). Climate change drives a much larger reduction in CO_2 uptake in the subpolar Southern Ocean in two of the four models (Fig. 8h and Fig. 5). In BCM-C, this is due to much greater local sea surface warming relative to the global increase in atmospheric temperature, while in MPIM it is due to the greater climate sensitivity α (K ppm^{-1}) of MPIM; that is, a greater change in global atmospheric temperature for a given change in atmospheric CO_2 (Table 3).

Previous studies have primarily focused on the North Atlantic (Crueger et al. 2008; Yoshikawa et al. 2008) and the Southern Ocean (Sarmiento and Le Quéré 1996; Sarmiento et al. 1998; Plattner et al. 2001; Crueger et al. 2008) as the key regions responsible for the global oceanic climate–carbon cycle feedback in the twenty-first century. In the studies of the oceanic climate–carbon cycle feedbacks where the linear feedback analysis has not been applied (Crueger et al. 2008; Yoshikawa et al.

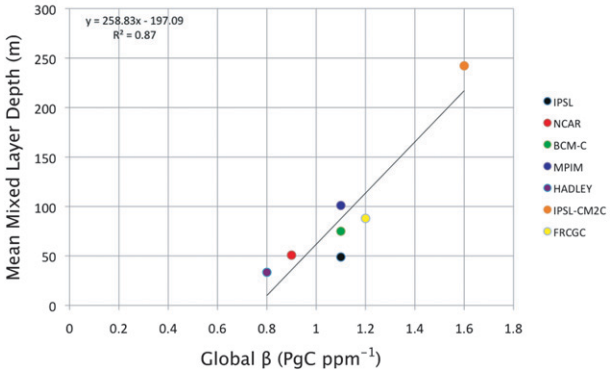

FIG. 9. The relationship between global-mean annual-mean mixed-layer depth (m) and global β (PgC ppm^{-1}) for some of the models used in Friedlingstein et al. (2006) and an additional model, BCM-C, over the time period 1860–2100.

2008; Tjiputra et al. 2010), the strength of the climate-induced reductions in CO_2 uptake from the equatorial and subpolar Southern Ocean have been underestimated. For example, the same MPIM simulations used here were used in Crueger et al. (2008); yet, they do not capture the large impact in the equatorial regions because they do not remove the ΔC_{CO2} due to the climate–carbon cycle feedbacks from the terrestrial biosphere—they subtract the uncoupled from the coupled simulation and assume that this difference in CO_2 uptake is due to the climate change impact on the ocean. The error $\varepsilon(\Delta C_{CO2})$ introduced by this approximation is

$$\varepsilon(\Delta C_{CO2}) = \beta(\Delta C_A^C - \Delta C_A^U) \qquad (10)$$

and produces the most significant impact where the regional βs are large: 9.7 PgC in the tropics (64% error) and 5.9 PgC in the subpolar Southern Ocean (48% error). Adjusting for this error increases the climate impact on the CO_2 fluxes within the Southern Ocean and the equatorial regions in this study relative to the study of Crueger et al. (2008). Similar underestimates of the climate impact on the CO_2 fluxes are expected in the studies that do not apply the regional linear feedback analysis (Yoshikawa et al. 2008; Tjiputra et al. 2010). Although Plattner et al. (2001) did not apply the linear feedback analysis approach, the equatorial regions were identified as a region of dominant anthropogenic CO_2 uptake. This is because—unlike in the C^{4}MIP simulations with climate–terrestrial carbon cycle coupling—subtracting the uncoupled from the coupled simulations of Plattner et al. (2001) does provide a good approximation of ΔC_{CLIM} because they do not simulate the large feedbacks caused by climate change on the terrestrial biosphere. It is mostly the reduction in CO_2 uptake by the terrestrial biosphere with global warming that increases atmospheric CO_2 in the coupled simulation relative to the uncoupled simulation in the C^{4}MIP simulations. Consequently, the trajectories of atmospheric CO_2 increase in the uncoupled and coupled simulations of Plattner et al. (2001) do not differ significantly, and the error [Eq. (10)] is small.

Other linear feedback analysis approaches have been recently developed to quantify climate–carbon cycle feedbacks (Boer and Arora 2009; Gregory et al. 2009). It has been demonstrated that in emissions scenarios with greater rates of atmospheric CO_2 increase, the magnitude of β is lower while γ is relatively insensitive. The atmospheric CO_2 concentrations at the end of the coupled C^{4}M simulations are higher than in the uncoupled simulations, yet the approach of Friedlingstein et al. (2006) assumes that the βs in both simulations are identical (see section 2c). This assumption causes an overestimation of the magnitudes of γ. A third simulation, a ''radiatively coupled'' one in which the CO_2 increase has no biogeochemical effect, is required to correct for this error in future studies (Gregory et al. 2009).

We apply the technique of Boer and Arora (2009) to the global model results and show that their technique does not give appreciably different estimates of ΔC_{CLIM} and ΔC_{CO2} (i.e., 168.9 ± 19.33 and −38.59 ± 10.7 respectively, compare with Tables 2 and 3). Both techniques work equally well at the global scale. However, we could expect that regional responses differ if we calculated the distribution of feedback parameters according to the approach of Boer and Arora (2010). They calculate regional feedback sensitivity parameters based on local CO_2 fluxes, atmospheric temperature, and CO_2 concentrations, while our local sensitivity parameters are calculated using globally averaged atmospheric temperature and CO_2 concentrations. The influence of local changes in atmospheric temperature and pCO_2 on the regional estimates of ΔC_{CO2}, ΔC_{CLIM}, and the evolution of oceanic CO_2 sink should be explored in future studies.

2) THE REGIONAL BALANCE BETWEEN CO_2-INDUCED AND CLIMATE-INDUCED ANTHROPOGENIC CO_2 UPTAKE

Future changes in regional oceanic CO_2 uptake depend on the relative responses of air–sea CO_2 flux to rising atmospheric CO_2, ΔC_{CO2}, and climate change ΔC_{CLIM}. Previous studies have suggested that the climate change impact on the oceanic CO_2 uptake becomes evident toward the end of the twenty-first century (Crueger et al. 2008; Yoshikawa et al. 2008). Focusing on some of the regions where climate change produces

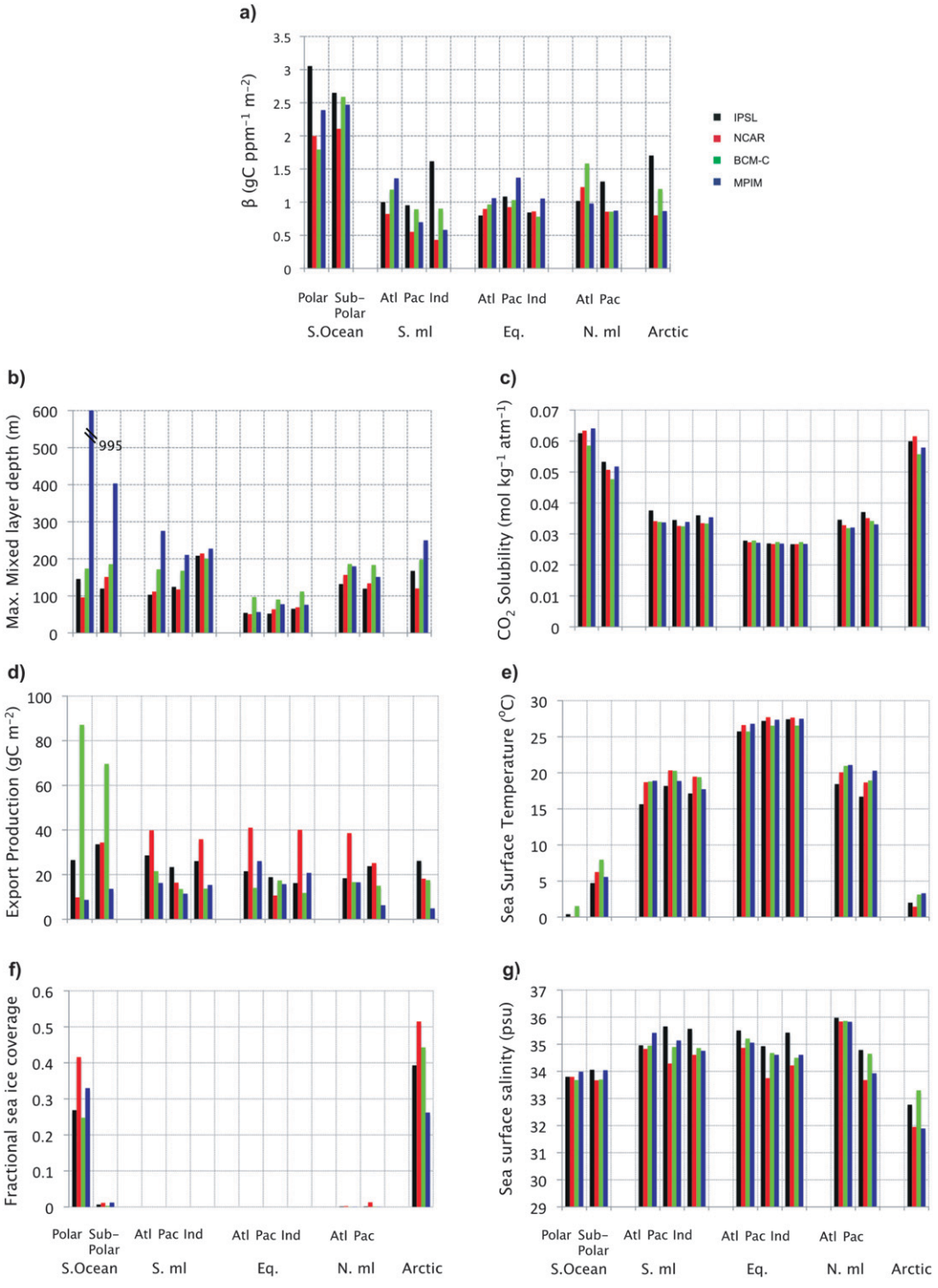

FIG. 10. (a) Regional β (gC ppm^{-1} m^{-2}). (b)–(g) Regionally averaged properties from the uncoupled C^{4}M simulations: (b) maximum mixed-layer depths (m); (c) CO_2 solubility (mol kg^{-1} atm^{-1}); (d) export production (gC m^{-2}); (e) sea surface temperature (°C); (f) fractional sea ice coverage; and (g) sea surface salinity (psu). Note that the definitions of export production vary between models, so a direct comparison is difficult (Schneider et al. 2008; Tjiputra et al. 2010). The regional averages were calculated over the 2010–2100 period with 10-yr smoothing. The regions are identical to those defined in Fig. 5.

TABLE 4. The AMOC in the C^4Ms. AMOC is defined as the maximum strength of the Atlantic overturning circulation at 30°N. The first column lists the time-averaged (1860–2010) AMOC for the uncoupled simulation, $AMOC^U$. The second column lists the difference in the change in the strength of the AMOC circulation between the coupled and uncoupled simulations, ΔAMOC; the change in the strength of the AMOC circulation is defined as the difference in the strength of the AMOC between the first (2000–2020) and last (2080–2100) 20 years. The third column lists the percent change in the AMOC rate [i.e., $(\Delta AMOC/AMOC^U) \times 100$].

Model	$AMOC^U$ [Sv (1 Sv $\equiv 10^6$ m^3 s^{-1})]	ΔAMOC (Sv)	Percentage change in AMOC
IPSL	13.4	−2.4	−18
NCAR	21.3	−1.8	−9
BCM-C	20.5	−2.8	−14
MPIM	19.3	−1.5	−8

larger impacts on the net anthropogenic CO_2 uptake, we show how ΔC_{CLIM} evolves relative to ΔC_{CO2} (Figs. 8i–l). The climate change impact on the CO_2 fluxes is already apparent at the beginning of this century. In fact, from the outset climate change reduces the CO_2-induced CO_2 uptake by a fixed proportion. Although climate change reduces the cumulated CO_2 uptake in the northern and southern extratropics by similar amounts (Table 2) in the IPSL model, this is enough to completely counteract the cumulated CO_2 uptake due to rising atmospheric CO_2 concentrations in the midlatitude North Atlantic (i.e., $C_{CLIM} > C_{CO2}$, Fig. 8i). In the northern extratropics, climate change reduces the CO_2-induced CO_2 uptake by approximately 50% (Table 2) and by only about 25% in the southern extratropics and equatorial regions (Table 2). Thus, these regions continue to dominate the anthropogenic CO_2 uptake by the global ocean beyond the end of this century.

The linearity between ΔC_{CLIM} and ΔC_{CO2} partly reflects our focus on the time-integrated oceanic CO_2 flux rather than the flux itself. Nevertheless, we expect a correlation between ΔC_{CLIM} and ΔC_{CO2} in C^4Ms. Oschlies (2009) quantified a 50% compensatory ''back flux'' from the surface ocean to the atmosphere in a C^4M model, when an increase in the biological pump reduces atmospheric CO_2 and subsequently decreases the efficiency of anthropogenic CO_2 uptake. Similarly, we expect that a regional reduction in anthropogenic CO_2 uptake due to climate change (negative ΔC_{CLIM}), which increases atmospheric CO_2, could be offset by an increase in oceanic CO_2 uptake due to a CO_2-induced ''return flux'' (positive ΔC_{CO2}).

The constant proportionality of the evolution of ΔC_{CLIM} relative to ΔC_{CO2} up until the end of the century would have several implications for quantifying the impact of climate change on oceanic CO_2 uptake. First, it would be difficult to detect the climate-induced component of change in cumulated CO_2 uptake based on CO_2 fluxes alone; other tracers, such as oxygen (Keeling et al. 1996; Matear and Hirst 2001, manuscript submitted to *G-cubed*; Bopp et al. 2002; Frölicher et al. 2009), would be required. Second, taking the ensemble global-mean $\Delta C_{CLIM}/\Delta C_{CO2}$ of approximately 0.25 and the cumulated CO_2 uptake of 118 ± 19 PgC (Sabine et al. 2004) would imply that climate change has already caused a reduction of approximately 40 PgC since the onset of anthropogenic CO_2 increase. Third, even if climate change does substantially impact the oceanic CO_2 uptake, our models do not simulate any strong nonlinearities in this effect up until the end of the twenty-first century. Recent observation-based studies suggest that the opposite may occur and that the rate of oceanic CO_2 uptake is not keeping up with the rate of increase in atmospheric CO_2 (Le Quere et al. 2007; Schuster and Watson 2007; Khatiwala et al. 2009; Lenton et al. 2009; Metzl 2009). It is possible that the observed reductions in the ocean's ability to sequester anthropogenic CO_2 may be driven by variability rather than long-term change. Also, there are several reasons why the C^4Ms may not represent the true evolution of the oceanic CO_2 uptake: (i) we do not include stratospheric ozone depletion–recovery in the simulations (Lenton et al. 2009), (ii) the C^4Ms do not capture nonlinear changes in CO_2 uptake that could occur in response to climate warming (Friedlingstein et al. 2006), and (iii) the models may be unable to adequately simulate the observed decadal–multidecadal changes since the C^4Ms produce their own internal variability. A rigorous comparison of simulated and observed annual air–sea CO_2 fluxes is necessary to understand this discrepancy.

Finally, in future studies intermodel comparisons of the stability of the regional feedback parameters, and the subsequent evolution of ΔC_{CLIM} relative to ΔC_{CO2}, under different emission scenarios should be conducted. It has been demonstrated that both the strength and evolution of the climate–carbon cycle feedbacks are sensitive to the emission scenario (Plattner et al. 2001; Boer and Arora 2009; Gregory et al. 2009). Yet, encouragingly, Boer and Arora (2010) found the distribution of both CO_2- and climate-sensitivity parameters to be comparatively robust across a range of emission scenarios.

5. Conclusions

Distributions of the sensitivity of oceanic CO_2 uptake (2010–2100) to rising atmospheric CO_2 concentrations (β) and climate change (γ) have been determined by applying the linear feedback analysis approach of

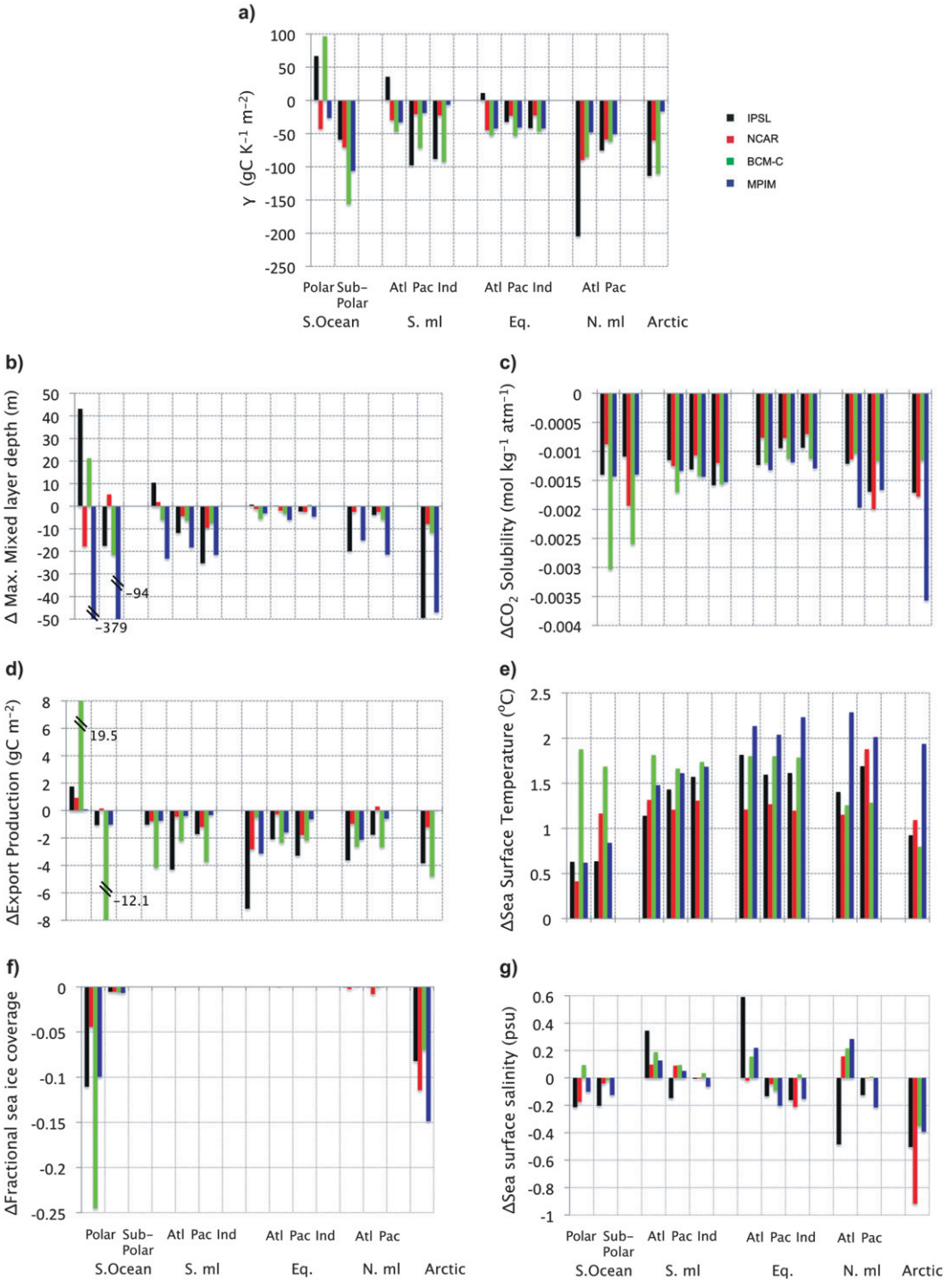

FIG. 11. As in Fig. 10, but for regional γ (gC K^{-1} m^{-2}) and (b)–(g) regionally averaged climate-induced changes in the selected C^4M properties.The changes are calculated by subtracting the first 10 years (2010–2020) from the last 10 years (2090–2100) of the difference between the coupled and uncoupled with 10-yr smoothing.

Friedlingstein et al. (2006) to the regional CO_2 fluxes simulated with coupled climate–cycle models (C^4Ms). The regional cumulated CO_2 fluxes have been separated into a CO_2-induced component (ΔC_{CO2}), due to rising atmospheric CO_2 concentrations, and a climate-induced component (ΔC_{CLIM}), due to climate change.

The regional impacts of rising atmospheric CO_2 concentrations on the simulated CO_2 uptake are well represented: (i) the C^4Ms simulate similar magnitudes and distributions of β, (ii) the global βs are similar to observation-based estimates (Sabine et al. 2004), and (iii) the regional distributions of β are broadly consistent with anthropogenic CO_2 uptake estimates from ocean inversions (Mikaloff-Fletcher et al. 2006) and forward model simulations (Orr et al. 2001).

Simulated climate change causes a $\Delta C_{CLIM} = 41.5 \pm 8.0$ PgC reduction in the global oceanic CO_2 sink by the end of this century, which offsets the $\Delta C_{CO2} = 170.7 \pm 17.4$ PgC increase in uptake due to rising atmospheric CO_2 concentrations and produces a positive climate–carbon cycle feedback on atmospheric CO_2 concentrations. The regional responses of the oceanic CO_2 uptake to climate change are broadly consistent between the models, with reduced CO_2 uptake due to decreases in solubility and increases in stratification in the midlatitudes and due to decreases in solubility in the subpolar Southern Ocean and the equatorial latitudes—the equatorial regions have been generally overlooked as an important contributor to the climate–carbon cycle feedback.

Anomalously strong climate-induced reductions in CO_2 uptake from the northern midlatitudes occur where ice calving produces large freshwater fluxes to the surface of the Atlantic Ocean; efforts to include a more realistic representation of high-latitude processes in the C^4Ms should improve simulations of the impact of climate change on CO_2 uptake within this region. In the southern extratropics, the CO_2 uptake is particularly sensitive to local warming; improvements in simulated Southern Ocean dynamics should increase our confidence in the future changes in CO_2 uptake here. In the equatorial regions, small changes in the temperature-induced CO_2 solubility can drive magnitudes and intermodel variability in the climate-induced CO_2 uptake that maybe larger than within the Southern Ocean; however, efforts to reduce the intermodel variability may be difficult since the uncertainty reflects relatively small differences in CO_2 solubility.

If the carbon cycle responds to climate warming as simulated by the C^4Ms, monitoring CO_2 fluxes alone may not be sufficient for the detection of the climate change impact on the oceanic anthropogenic CO_2 carbon uptake in the future; regional changes in atmospheric and oceanic oxygen should be monitored in parallel.

Future studies should include as many of the C^4Ms currently used in the scientific community as possible and draw on larger selection of diagnostics, particularly of the ocean circulation (i.e., CFCs, vertical diffusivities, wind stress, and sea surface height). Systematic sensitivity tests (Plattner et al. 2001) would help identify the aspects of the oceanic carbon cycle that are expected to dominate the regional climate–carbon cycle feedbacks from the ocean. We should develop more sophisticated Lagrangian and Eulerian approaches (Iudicone et al. 2008a,b) to rigorously track and quantify the impact of climate change on anthropogenic CO_2 taken up via various circulation pathways in the C^4Ms and to understand the role of ocean dynamics on the climate–carbon cycle feedbacks from the ocean. In parallel to the studies of the future climate–carbon cycle feedbacks, it is essential that we validate the trends in anthropogenic CO_2 uptake simulated by the C^4Ms over the historical period using the available observational databases; in regions with sufficient ΔpCO_2 observations, a model–data comparison of the trends in ΔpCO_2 should make it possible to assess the sign, the magnitude, and the drivers of the simulated ΔpCO_2 trends.

Acknowledgments. This work was supported by the European Commission through EU FP6 Integrated Project CARBOOCEAN (Contract No. 511176). Work by Uib/BCCR was supported by the Norwegian Research Council NFR through projects CarboSeason (185105/S30) and NorCLIM (178246/S30) of the NORKLIMA programme and through supercomputing project nn2980k of the Norwegian Metacenter for Computational Science (NOTUR). Work by LSCE was supported by IDRIS/CCRT supercomputing centers. Computational resources for the UNIBE simulations were provided by the Swiss National Supercomputing Centre (CSCS).

REFERENCES

Aumont, O., and L. Bopp, 2006: Globalizing results from ocean in situ iron fertilization studies. *Global Biogeochem. Cycles,* **20,** GB2017, doi:10.1029/2005GB002591.

——, E. Maier-Reimer, S. Blain, and P. Monfray, 2003: An ecosystem model of the global ocean including Fe, Si, P colimitations. *Global Biogeochem. Cycles,* **17,** 1060, doi:10.1029/2001GB001745.

Bates, N. R., S. B. Moran, D. A. Hansell, and J. T. Mathis, 2006: An increasing CO_2 sink in the Arctic Ocean due to sea-ice loss. *Geophys. Res. Lett.,* **33,** L23609, doi:10.1029/2006GL027028.

Bleck, R., C. Rooth, D. M. Hu, and L. T. Smith, 1992: Salinity-driven thermocline transients in a wind-forced and thermohaline-forced isopycnic coordinate model of the North Atlantic. *J. Phys. Oceanogr.,* **22,** 1486–1505.

Boer, G. J., and V. Arora, 2009: Temperature and concentration feedbacks in the carbon cycle. *Geophys. Res. Lett.,* **36,** L02704, doi:10.1029/2008GL036220.

——, and ——, 2010: Geographic aspects of temperature and concentration feedbacks in the carbon budget. *J. Climate,* **23,** 775–784.

Bopp, L., C. Le Quere, M. Heimann, A. C. Manning, and P. Monfray, 2002: Climate-induced oceanic oxygen fluxes: Implications for the contemporary carbon budget. *Global Biogeochem. Cycles,* **16,** 1022, doi:10.1029/2001GB001445.

Boville, B. A., and P. R. Gent, 1998: The NCAR Climate System Model, version one. *J. Climate,* **11,** 1115–1130.

——, J. T. Kiehl, P. J. Rasch, and F. O. Bryan, 2001: Improvements to the NCAR CSM-1 for transient climate simulations. *J. Climate,* **14,** 164–179.

Boyer-Montegut, C. D., G. Madec, A. S. Fischer, A. Lazar, and D. Iudicone, 2004: Mixed layer depth over the global ocean: An examination of profile data and a profile-based climatology. *J. Geophys. Res.,* **109,** C12003, doi:10.1029/2004JC002378.

Collier, M. A., and P. Durack, 2006: CSIRO netCDF version of the NODC World Ocean Atlas 2005. Commonwealth Scientific and Industrial Research Organisation, Marine and Atmospheric Research Paper 15, 1–45 pp.

Conkright, M. E., R. A. Locarnini, H. E. Garcia, T. D. O'Brien, T. P. Boyer, B. B. Stephens, and J. I. Antonov, 2002: *World Ocean Atlas 2001: Objective Analyses, Data, Statistics, and Figures. CD-ROM Documentation*. National Oceanographic Data Center, 17 pp.

Cox, P. M., R. A. Betts, C. D. Jones, S. A. Spall, and I. J. Totterdell, 2000: Acceleration of global warming due to carbon cycle feedbacks in a coupled climate model. *Nature,* **408,** 184–187.

——, ——, M. Collins, P. P. Harris, C. Huntingford, and C. D. Jones, 2004: Amazonian forest dieback under climate–carbon cycle projections for the 21st century. *Theor. Appl. Climatol.,* **78,** 137–156.

Crueger, T., E. Roeckner, T. Raddatz, R. Schnur, and P. Wetzel, 2008: Ocean dynamics determine the response of oceanic CO_2 uptake to climate change. *Climate Dyn.,* **31,** 151–168.

Deque, M., C. Dreveton, A. Braun, and D. Cariolle, 1994: The ARPEGE/IF's atmosphere model—A contribution to the French community climate modeling. *Climate Dyn.,* **10,** 249–266.

Doney, S. C., K. Lindsay, I. Fung, and J. John, 2006: Natural variability in a stable, 1000-yr global coupled climate–carbon cycle simulation. *J. Climate,* **19,** 3033–3054.

Dufresne, J. L., and Coauthors, 2002: On the magnitude of positive feedback between future climate change and the carbon cycle. *Geophys. Res. Lett.,* **29,** 1405, doi:10.1029/2001GL013777.

Dutay, J.-C., and Coauthors, 2002: Evaluation of ocean model ventilation with CFC-11: Comparison of 13 global ocean models. *Ocean Modell.,* **4,** 89–120.

Edmonds, J. A., F. Joos, N. Nakicenovic, R. G. Richels, and J. L. Sarmiento, 2004: Scenarios, targets, gaps, and costs. *The Global Carbon Cycle. Integrating Humans, Climate, and the Natural World,* C. B. Field, and M. R. Raupach, Eds., Island Press, 77–102.

Friedlingstein, P., L. Bopp, P. Ciais, J.-L. Dufresne, L. Fairhead, H. LeTreut, P. Monfray, and J. Orr, 2001: Positive feedback between future climate change and the carbon cycle. *Geophys. Res. Lett.,* **28,** 1543–1546.

——, and Coauthors, 2006: Climate–carbon cycle feedback analysis: Results from the (CMIP)-M-4 model intercomparison. *J. Climate,* **19,** 3337–3353.

Frölicher, T. L., and F. Joos, 2010: Reversible and irreversible impacts of greenhouse gas emissions in multi-century projections with the NCAR global coupled carbon cycle-climate model. *Climate Dyn.,* **35,** 1439–1459.

——, ——, G. K. Plattner, M. Steinacher, and S. C. Doney, 2009: Natural variability and anthropogenic trends in oceanic oxygen in a coupled carbon cycle-climate model ensemble. *Global Biogeochem. Cycles,* **23,** GB1003, doi:10.1029/2008GB003316.

Fung, I. Y., S. C. Doney, K. Lindsay, and J. John, 2005: Evolution of carbon sinks in a changing climate. *Proc. Natl. Acad. Sci. USA,* **102,** 11 201–11 206.

Furevik, T., M. Bentsen, H. Drange, I. K. T. Kindem, N. G. Kvamsto, and A. Sorteberg, 2003: Description and evaluation of the bergen climate model: ARPEGE coupled with MICOM. *Climate Dyn.,* **21,** 27–51.

Gehlen, M., L. Bopp, N. Ernprin, O. Aumont, C. Heinze, and O. Raguencau, 2006: Reconciling surface ocean productivity, export fluxes and sediment composition in a global biogeochemical ocean model. *Biogeosciences,* **3,** 521–537.

Gent, P. R., F. O. Bryan, G. Danabasoglu, S. C. Doney, W. R. Holland, W. G. Large, and J. C. McWilliams, 1998: The NCAR climate system model global ocean component. *J. Climate,* **11,** 1287–1306.

Gerber, M., and F. Joos, 2010: Carbon sources and sinks from an ensemble Kalman filter ocean data assimilation. *Global Biogeochem. Cycles,* **24,** GB3004, doi:10.1029/2009GB003531.

——, ——, M. Vázquez-Rodriguez, F. Touratier, and C. Goyet, 2009: Regional air–sea fluxes of anthropogenic carbon inferred with an ensemble Kalman filter. *Global Biogeochem. Cycles,* **23,** GB1013, doi:10.1029/2008GB003247.

Gregory, J. M., C. D. Jones, P. Cadule, and P. Friedlingstein, 2009: Quantifying carbon cycle feedbacks. *J. Climate,* **22,** 5232–5250.

Gruber, N., and Coauthors, 2009: Oceanic sources, sinks, and transport of atmospheric CO_2. *Global Biogeochem. Cycles,* **23,** GB1005, doi:10.1029/2008GB003349.

Hourdin, F., and Coauthors, 2006: The LMDZ4 general circulation model: Climate performance and sensitivity to parametrized physics with emphasis on tropical convection. *Climate Dyn.,* **27,** 787–813.

Ito, T., M. Woloszyn, and M. Mazloff, 2010: Anthropogenic carbon dioxide transport in the Southern Ocean driven by Ekman flow. *Nature,* **463,** 80–83.

Iudicone, D., G. Madec, B. Blanke, and S. Speich, 2008a: The role of Southern Ocean surface forcings and mixing in the global conveyor. *J. Phys. Oceanogr.,* **38,** 1377–1400.

——, ——, and T. J. McDougall, 2008b: Water-mass transformations in a neutral density framework and the key role of light penetration. *J. Phys. Oceanogr.,* **38,** 1357–1376.

Jacobson, A. R., S. E. M. Fletcher, N. Gruber, J. L. Sarmiento, and M. Gloor, 2007: A joint atmosphere-ocean inversion for surface fluxes of carbon dioxide: 2. Regional results. *Global Biogeochem. Cycles,* **21,** GB1020, doi:10.1029/2006GB002703.

Jones, C. D., P. Cox, and C. Huntingford, 2003: Uncertainty in climate–carbon cycle projections associated with the sensitivity of soil respiration to temperature. *Tellus,* **55B,** 642–648.

——, P. M. Cox, and C. Huntingford, 2006: Climate–carbon cycle feedbacks under stabilization: Uncertainty and observational constraints. *Tellus,* **58B,** 603–613.

Joos, F., G.-K. Plattner, T. F. Stocker, O. Marchal, and A. Schmittner, 1999: Global warming and marine carbon cycle feedbacks on future atmospheric CO_2. *Science,* **284,** 464–476.

——, and Coauthors, 2001: Global warming feedbacks on terrestrial carbon uptake under the Intergovernmental Panel on Climate Change (IPCC) emission scenarios. *Global Biogeochem. Cycles,* **15,** 891–907.

Keeling, R. F., S. C. Piper, and M. Heimann, 1996: Global and hemispheric CO_2 sinks deduced from changes in atmospheric O_2 concentrations. *Nature,* **381,** 218–221.

Key, R. M., and Coauthors, 2004: A global ocean carbon climatology: Results from Global Data Analysis Project (GLODAP). *Global Biogeochem. Cycles,* **18,** GB4031, doi:10.1029/2004GB002247.

Khatiwala, S., F. Primeau, and T. Hall, 2009: Reconstruction of the history of anthropogenic CO_2 concentrations in the ocean. *Nature,* **462,** 346–U110.

Kiehl, J. T., J. J. Hack, G. B. Bonan, B. A. Boville, D. L. Williamson, and P. J. Rasch, 1998: The National Center for Atmospheric Research Community Climate Model: CCM3. *J. Climate,* **11,** 1131–1149.

Krinner, G., and Coauthors, 2005: A dynamic global vegetation model for studies of the coupled atmosphere-biosphere system. *Global Biogeochem. Cycles,* **19,** GB1015, doi:10.1029/2003GB002199.

Lachkar, Z., J. C. Orr, J. C. Dutay, and P. Delecluse, 2009: On the role of mesoscale eddies in the ventilation of Antarctic intermediate water. *Deep-Sea Res. I,* **56,** 909–925.

Lenton, A., F. Codron, L. Bopp, N. Metzl, P. Cadule, A. Tagliabue, and J. Le Sommer, 2009: Stratospheric ozone depletion reduces ocean carbon uptake and enhances ocean acidification. *Geophys. Res. Lett.,* **36,** L12606, doi:10.1029/2009GL038227.

Le Quere, C., and Coauthors, 2007: Saturation of the Southern Ocean CO_2 sink due to recent climate change. *Science,* **319,** 1735–1738.

Levitus, S., 1982: *Climatological Atlas of the World Ocean*. NOAA Prof. Paper 13, 173 pp. and 17 microfiche.

——, and T. P. Boyer, 1994: *Temperature*. Vol. 4, *World Ocean Atlas 1994,* NOAA Atlas NESDIS 4, 117 pp.

——, R. Burgett, and T. P. Boyer, 1994: *Salinity*. Vol. 3, *World Ocean Atlas 1994,* NOAA Atlas NESDIS 3, 99 pp.

——, M. E. Conkright, J. L. Reid, and R. G. Najjar, 1993: Distribution of nitrate, phosphate and silicate in the world oceans. *Prog. Oceanogr.,* **31,** 245–273.

Madec, G., P. Delecluse, M. Imbard, and M. Lévy, 1998: OPA 8.1 ocean general circulation model reference manual. Notes du Pôle de Modélisation 11. IPSL, 91 pp.

Maier-Reimer, E., 1993: Geochemical cycles in an Ocean General Circulation Model. Preindustrial tracer distributions. *Global Biogeochem. Cycles,* **7,** 645–677.

——, U. Mikolajewicz, and K. Hasselmann, 1993: Mean circulation of the Hamburg LSG OGCM and its sensitivity to the thermohaline surface forcing. *J. Phys. Oceanogr.,* **23,** 769–782.

——, ——, and A. Winguth, 1996: Future ocean uptake of CO_2: Interaction between ocean circulation and biology. *Climate Dyn.,* **12,** 711–721.

——, I. Kriest, J. Segschneider, and P. Wezel, 2005: The Hamburg Ocean Carbon Cycle model HAMOCC5.1—Technical Description. Tech. Description Release 1.1, Berichte zur Erdsystemforschung 14, Max Planck Institute for Meteorology, 50 pp.

Marland, G., and T. B. R. J. Andres, 2005: Global, regional, and national CO_2 emissions. *Trends: A Compendium of Data on Global Change,* Information Analysis Center, Oak Ridge National Laboratory, U.S. Department of Energy.

Marsland, S. J., H. Haak, J. H. Jungclaus, M. Latif, and F. Roske, 2003: The Max Planck Institute global ocean/sea ice model with orthogonal curvilinear coordinates. *Ocean Modell.,* **5,** 91–127.

Marti, O., and Coauthors, 2009: Key features of the IPSL ocean atmosphere model and its sensitivity to atmospheric resolution. *Climate Dyn.,* **34,** 1–26.

Matear, R. J., and A. C. Hirst, 1999: Climate change feedback on the future oceanic CO_2 uptake. *Tellus,* **51B,** 722–733.

Matsumoto, K., and Coauthors, 2004: Evaluation of ocean carbon cycle models with data-based metrics. *Geophys. Res. Lett.,* **31,** L07303, doi:10.1029/2003GL018970.

Matthews, H. D., 2006: Emissions targets for CO_2 stabilization as modified by carbon cycle feedbacks. *Tellus,* **58B,** 591–602.

——, 2007: Implications of CO_2 fertilization for future climate change in a coupled climate–carbon model. *Global Change Biol.,* **13,** 1068–1078.

——, and D. W. Keith, 2007: Carbon-cycle feedbacks increase the likelihood of a warmer future. *Geophys. Res. Lett.,* **34,** L09702, doi:10.1029/2006GL028685.

——, M. Eby, A. J. Weaver, and B. J. Hawkins, 2005: Primary productivity control of simulated carbon cycle-climate feedbacks. *Geophys. Res. Lett.,* **32,** L14708, doi:10.1029/2005GL022941.

——, ——, T. Ewen, P. Friedlingstein, and B. J. Hawkins, 2007: What determines the magnitude of carbon cycle-climate feedbacks? *Global Biogeochem. Cycles,* **21,** GB2012, doi:10.1029/2006GB002733.

Meehl, G., and Coauthors, 2007: Global climate projections. *Climate Change 2007: The Physical Science Basis,* S. Solomon et al., Eds., Cambridge University Press, 747–846.

Metzl, N., 2009: Decadal increase of oceanic carbon dioxide in Southern Indian Ocean surface waters (1991-2007). *Deep-Sea Res. II,* **56,** 607–609.

Meyer, R., and Coauthors, 1999: The substitution of high-resolution terrestrial biosphere models and carbon sequestration in response to changing CO_2 and climate. *Global Biogeochem. Cycles,* **13,** 785–802.

Mignone, B. K., A. Gnanadesikan, J. L. Sarmiento, and R. D. Slater, 2006: Central role of Southern Hemisphere winds and eddies in modulating the oceanic uptake of anthropogenic carbon. *Geophys. Res. Lett.,* **33,** L01604, doi:10.1029/2005GL024464.

Mikaloff-Fletcher, S. E. M., and Coauthors, 2006: Inverse estimates of anthropogenic CO_2 uptake, transport, and storage by the ocean. *Global Biogeochem. Cycles,* **20,** GB2002, doi:10.1029/2005GB002530.

Najjar, R. G., and Coauthors, 2007: Impact of circulation on export production, dissolved organic matter, and dissolved oxygen in the ocean: Results from Phase II of the Ocean Carbon-cycle Model Intercomparison Project (OCMIP-2). *Global Biogeochem. Cycles,* **21,** GB3007, doi:10.1029/2006GB002857.

Nakicenovic, N., and Coauthors, 2000: *IPCC Special Report on Emission Scenarios*. Cambridge University Press, 599 pp.

Orr, J. C., and Coauthors, 2001: Estimate of anthropogenic carbon uptake from four three-dimensional global models. *Global Biogeochem. Cycles,* **15,** 43–60.

Oschlies, A., 2009: Impact of atmospheric and terrestrial CO_2 feedbacks on fertilization-induced marine carbon uptake. *Biogeosciences,* **6,** 1603–1613.

Plattner, G. K., F. Joos, T. F. Stocker, and O. Marchal, 2001: Feedback mechanisms and sensitivities of ocean carbon uptake under global warming. *Tellus,* **53B,** 564–592.

Prentice, I. C., and Coauthors, 2001: The carbon cycle and atmospheric carbon dioxide. *Climate Change 2001: The Scientific Basis,* J. T. Houghton, et al., Eds., Cambridge University Press, 183–237.

Randerson, J. T., M. V. Thompson, T. J. Conway, I. Y. Fung, and C. B. Field, 1997: The contribution of terrestrial sources and sinks to trends in the seasonal cycle of atmospheric carbon dioxide. *Global Biogeochem. Cycles,* **11,** 535–560.

Roeckner, E., J. M. Oberhuber, A. Bacher, M. Christoph, and I. Kirchner, 1996: ENSO variability and atmospheric response in a global coupled atmosphere-ocean GCM. *Climate Dyn.,* **12,** 737–754.

Sabine, C. L., and Coauthors, 2004: The oceanic sink for anthropogenic CO_2. *Science,* **305,** 367–371.

Sarmiento, J. L., and C. Le Quéré, 1996: Oceanic carbon dioxide uptake in a model of century-scale global warming. *Science,* **274,** 1346–1350.

——, T. M. C. Hughes, R. J. Stouffer, and S. Manabe, 1998: Simulated response of the ocean carbon cycle to anthropogenic climate warming. *Nature,* **393,** 245–249.

Schneider, B., and Coauthors, 2008: Climate-induced interannual variability of marine primary and export production in three global coupled climate carbon cycle models. *Biogeosciences,* **5,** 597–614.

Schuster, U., and A. J. Watson, 2007: A variable and decreasing sink for atmospheric CO_2 in the North Atlantic. *J. Geophys. Res.,* **112,** C11006, doi:10.1029/2006JC003941.

——, and Coauthors, 2009: Trends in North Atlantic sea surface fCO_2 from 1990 to 2006. *Deep-Sea Res. II,* **56,** 620–629.

Sitch, S., and Coauthors, 2003: Evaluation of ecosystem dynamics, plant geography and terrestrial carbon cycling in the LPJ dynamic global vegetation model. *Global Change Biol.,* **9,** 161–185.

Six, K. D., and E. Maier-Reimer, 1996: Effects of plankton dynamics on seasonal carbon fluxes in an ocean general circulation model. *Global Biogeochem. Cycles,* **10,** 559–583.

Steinacher, M., F. Joos, T. L. Frolicher, G. K. Plattner, and S. C. Doney, 2009: Imminent ocean acidification in the Arctic projected with the NCAR global coupled carbon cycle-climate model. *Biogeosciences,* **6,** 515–533.

——, and Coauthors, 2010: Projected 21st century decrease in marine productivity: a multi-model analysis. *Biogeosciences,* **7,** 979–1005.

Swingedouw, D., L. Bopp, A. Matras, and P. Braconnot, 2007: Effect of land-ice melting and associated changes in the AMOC result in little overall impact on oceanic CO_2 uptake. *Geophys. Res. Lett.,* **34,** L23706, doi:10.1029/2007GL031990.

Takahashi, T., and Coauthors, 2002: Global sea-air CO_2 flux based on climatological surface ocean pCO(2), and seasonal biological and temperature effects. *Deep-Sea Res. II,* **49,** 1601–1622.

——, and Coauthors, 2009: Climatological mean and decadal change in surface ocean pCO(2), and net sea-air CO_2 flux over the global oceans. *Deep-Sea Res. II,* **56,** 554–577.

Tjiputra, J. F., K. Assmann, M. Bentsen, I. Bethke, O. H. Ottera, C. Sturm, and C. Heinze, 2010: Bergen earth system model (BCM-C): Model description and regional climate–carbon cycle feedbacks assessment. *Geosci. Model Dev. Discuss.,* **2,** 845–887.

Watson, A. J., and Coauthors, 2009: Tracking the variable north atlantic sink for atmospheric CO_2. *Science,* **326,** 1391–1393.

Yoshikawa, C., M. Kawamiya, T. Kato, Y. Yamanaka, and T. Matsuno, 2008: Geographical distribution of the feedback between future climate change and the carbon cycle. *J. Geophys. Res.,* **113,** G03002, doi:10.1029/2007JG000570.